Materials Transactions, Vol. 43, No. 11 (2002) pp. 2678 to 2684
Special Issue on Protium New Function in Materials

Fabrication of Lotus-type Porous Stainless Steel by Unidirectional Solidification under Hydrogen Atmosphere

Teruyuki Ikeda, Michiharu Tsukamoto * and Hideo Nakajima

The Institute of Scientific and Industrial Research, Osaka University, Ibaraki 567-0047, Japan

Lotus-type porous stainless steel SUS304L has been fabricated by unidirectional solidification under mixed gases of hydrogen and argon. The atmospheric pressure dependence of porosity and pore diameter has been investigated. The porosity is lower if the partial pressure of argon is higher under a constant partial pressure of hydrogen and is higher if the partial pressure of hydrogen is higher under a constant total pressure of atmosphere composing of hydrogen and argon. Average pore diameter increases with increasing distance from the bottom chill plane. From tensile tests, the ultimate tensile strength of the porous stainless steel with porosity about 50% has been found to be about 7 times lower than nonporous alloy in the direction perpendicular to pore growth direction.

(Received July 22, 2002; Accepted September 9, 2002)

Keywords: *porous metal, stainless steel, tensile strength*

1. Introduction

Recently, porous and foamed metals and alloys have attracted much attentions, which exhibit some superior physical properties for application to light weight materials, damping materials and so on. Various fabrication methods of the porous and foamed metals and alloys were developed. For example, those are a foaming method with gas bubbling, an electroplating method for metal deposit in polyurethane form, a powder sintering metallurgy method and so on.[1–3] Usually the pores evolved in such porous metals are spherical and randomly distributed. On the other hand, formation of elongated gas pores during solidification of metals and alloys were studied by several investigators.[4–10] Recently, Nakajima and co-workers[10–24] investigated the fabrication of various porous metals and alloys with elongated pores in pressurised hydrogen, nitrogen or oxygen by a unidirectional solidification method. In order to distinguish the porous metals with elongated directional pores from sintered and foamed metals with rather spherical pores, we designate them lotus-type porous metals, because they look like lotus roots.

It was found that the lotus-type porous metals exhibit superior mechanical properties[18–20,24,25] and large internal friction.[26] Very recently, golf putter using lotus-type porous copper has been commercialised.[27] Thus, industrial application has been expected to expand to various fields. From the point of basic materials science, the porous metals are very interesting materials which would potentially exhibit novel various properties.

The present work has been undertaken to develop the fabrication method of lotus-type porous stainless steel (SUS304L), which is a practically important material in various applications. Moreover, the mechanical property of porous stainless steel has also been investigated in the present work.

*Present address: Mizuno Corp., Osaka 559-8510, Japan.

2. Experimental Procedure

2.1 Fabrication of porous stainless steel

The fabrication apparatus of the porous stainless steel consists of an alumina crucible surrounded by an induction-heating coil and a mold with water-cooled bottom copper plate. These are installed in a high pressure chamber. The detailed description was shown in Ref. 18).

Alloy pieces of SUS304L of about 100 g in weight were put into a crucible of alumina of 30 mm in diameter and 90 mm height (CP-2, Nikkato Corp.), which was dried well in air at 423 K for at least 3.6×10^3 s. The chemical composition of the alloy is shown in Table 1. The alloy was melted by high frequency induction heating in vacuum less than 6×10^{-3} Pa. Then hydrogen and argon gases were introduced into the chamber to a given pressure and the molten alloy was held at 1923 K for 6.0×10^2 s to make hydrogen gas be absorbed into the melt. The gas pressures of hydrogen and argon in this procedure are listed in Table 2. The temperature was measured using an infrared radiation thermometer (model IR-AP, Chino Corp.). The alloy was cast into the mold. Figure 1(a) shows a schematic picture of the mold. The bottom is of a water-cooled copper plate. The side wall is of a molybdenum sheet of 0.1 mm in thickness; solidification from the side wall is avoided by using the thin sheet with small heat capacity. The inner surface of the side wall is coated with alumina powder to avoid the reaction between the melt of alloy and the molybdenum sheet. Thus, the mold is designed for the solidification to occur vertically to the bottom plane.

The samples was cut in halves with a spark-erosion wire cutter in order to observe the structure of the cross sectional plane parallel to the solidification direction. Then a half piece was cut into disks of 1 or 2 mm in thickness; the cut plane is perpendicular to the solidification direction. Each surface was polished with a series of emery papers. The cross sections were observed with an optical microscope. In order to determine the porosity in each cross section perpendicular to the solidification direction, the area fractions of pores were analysed using a personal computer with an image processing program (Macscope, Mitani Corp.).

Table 1 Chemical composition of master ingot of SUS304L.

Element	C	Si	Mn	P	S	Cr	Ni	Cu	N	O	H
Concentration (mass%)	0.24	0.49	0.87	0.027	0.008	18.25	9.19	0.26	0.057	0.005	0.0004

Table 2 Pressures of hydrogen and argon during melting at 1923 K for 6.0×10^2 s before casting.

Ingot	H_2 pressure/MPa	Ar pressure/MPa	Total pressure/MPa
A	0.6	0	0.6
B	0.6	0.6	1.2
C	0.6	1.0	1.6
D	0.6	1.4	2.0
E	0	2.0	2.0
F	0.8	1.2	2.0
G	1.0	1.0	2.0
H	1.2	0.8	2.0
I	2.0	0	2.0

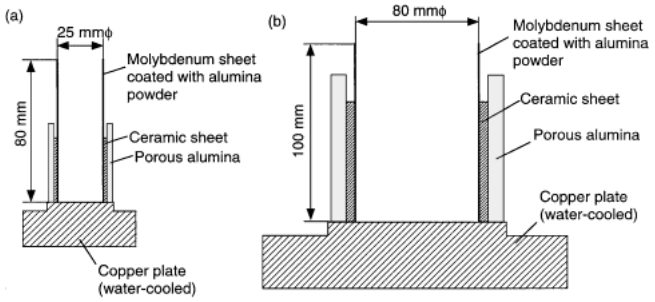

Fig. 1 Schematic pictures of the molds: (a) small ingots of porous stainless steel for investigating the structures and (b) larger ingots for preparing samples for tensile tests.

2.2 Tensile tests

Alloy pieces of about 1500 g were prepared in order to fabricate large ingots to cut out specimens for tensile tests. They were put into a crucible of alumina of 65 mm in diameter and 120 mm in height. The chamber was evacuated into vacuum less than 3×10^{-3} Pa. Then the alloy was melted by high frequency induction heating and held at 1923 K for 6.0×10^2 s under the atmosphere listed in Table 3. The alloy was cast into the mold shown in Fig. 1(b). The specimens for tensile tests shown in Fig. 2 have been cut out with a spark-erosion wire cutter. The tensile direction is perpendicular to the solidification direction, *i.e.* pore growth direction. The tensile tests have been performed at room temperature with an universal test machine (Model 4482, Instron Co. Ltd.). The crosshead speed was set up to be 0.1 mms^{-1}. The strains were detected by an extension meter with the gauge length of 11.5 mm.

3. Results and Discussion

3.1 Gas porosity

Figure 3 shows the cross sectional planes parallel and perpendicular to the solidification direction of the sample cast under the atmosphere of the mixture gas with hydrogen 1.0 MPa and argon 1.0 MPa (ingot 'G'). It is observed that a

Table 3 Pressures of hydrogen and argon during melting at 1923 K for 6.0×10^2 s. The ingots were cut out for tensile test specimens.

Ingot	H_2 pressure/MPa	Ar pressure/MPa	Total pressure/MPa
J	0	0.2	0.2
K	1.5	1.0	2.5

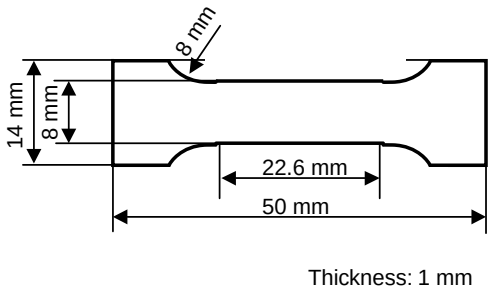

Fig. 2 Sample shape used for tensile tests.

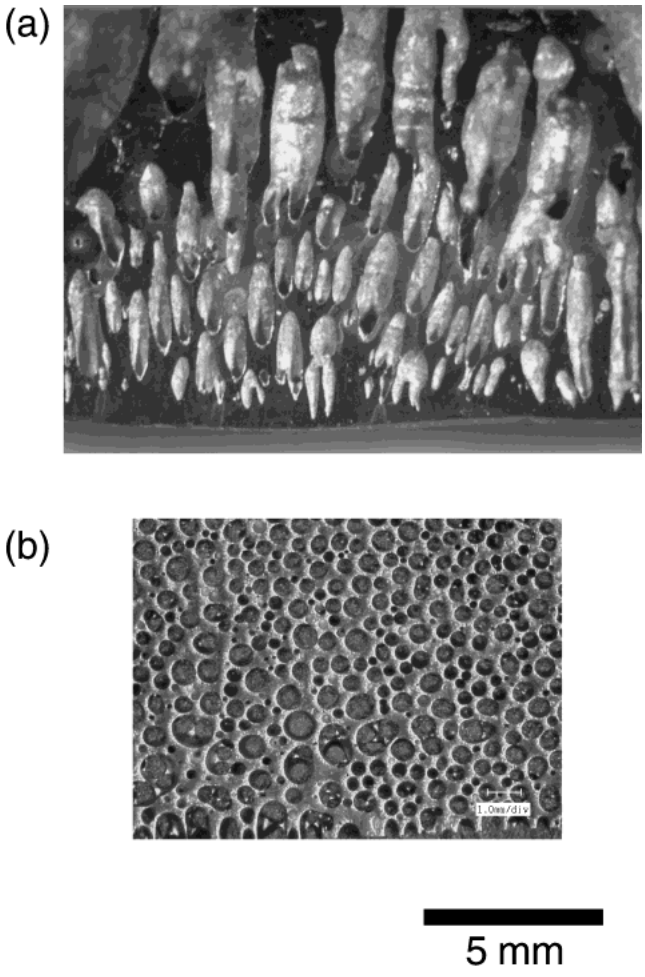

Fig. 3 Cross sectional planes (a) parallel and (b) perpendicular to the solidification direction in the ingot 'G', which was cast under mixture gas of 1.0 MPa of hydrogen and 1.0 MPa of argon.

lot of small pores in cylindrical shape extends in the solidification direction. The distribution of the pores in the cross section perpendicular to the solidification direction is almost homogeneous. On the other hand, the pores are not observed in the sample cast under argon gas of 2.0 MPa without hydrogen (ingot 'E'). Thus, the pores are considered to be evolved by hydrogen gas. It is necessary to the pore evolution that the solubility of gas atoms in the liquid state is larger than that in the solid state; there is a solubility gap at the melting temperature. Figure 4 shows the temperature dependence of the hydrogen solubility in Fe–18Cr–8Ni alloy.[28–30] Although the solubility in the vicinity of the melting temperature has not been reported, it is deduced, in this study, from the formation of pores in the ingots cast under hydrogen atmosphere that there is a solubility gap of hydrogen atoms between the solid state and liquid state.

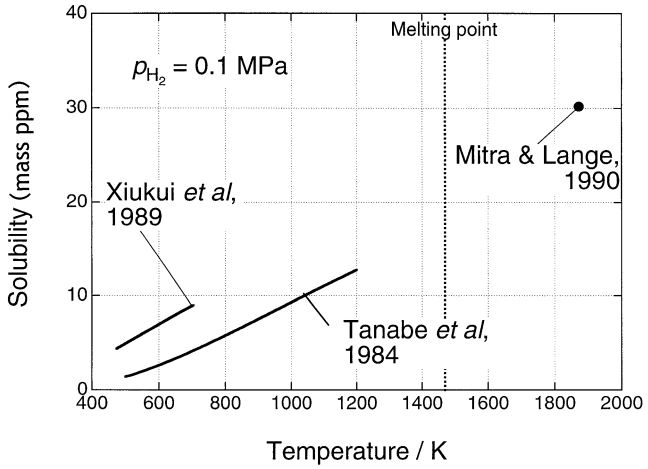

Fig. 4 Temperature dependence of hydrogen solubility in liquid[28,29] and solid[30] states of Fe–18Cr–8Ni alloy under hydrogen pressure 0.1 MPa.

3.2 Effect of partial pressure of argon on porosity

Figure 5 shows the cross sectional planes parallel to the solidification direction of the sample cast under hydrogen gas of 0.6 MPa mixed with various pressures of argon. It is observed that the pores grow larger in the sample cast under hydrogen of 0.6 MPa without argon than those in other samples cast under atmosphere with argon. In the samples cast using 0.6 MPa or 1.0 MPa of argon, the pores in cylindrical shape are observed to extend in the solidification direction. There are fewer pores in the sample fabricated with 1.4 MPa of argon than in the samples fabricated with 0.6 MPa or 1.0 MPa of argon. Figure 6 shows the porosity and average pore diameter as functions of the distance from the bottom plane determined by analysing the cross sections perpendicular to the solidification direction in the samples fabricated under 0.6 MPa of hydrogen and 1.0 MPa (sample C) or 1.4 MPa (sample D) of

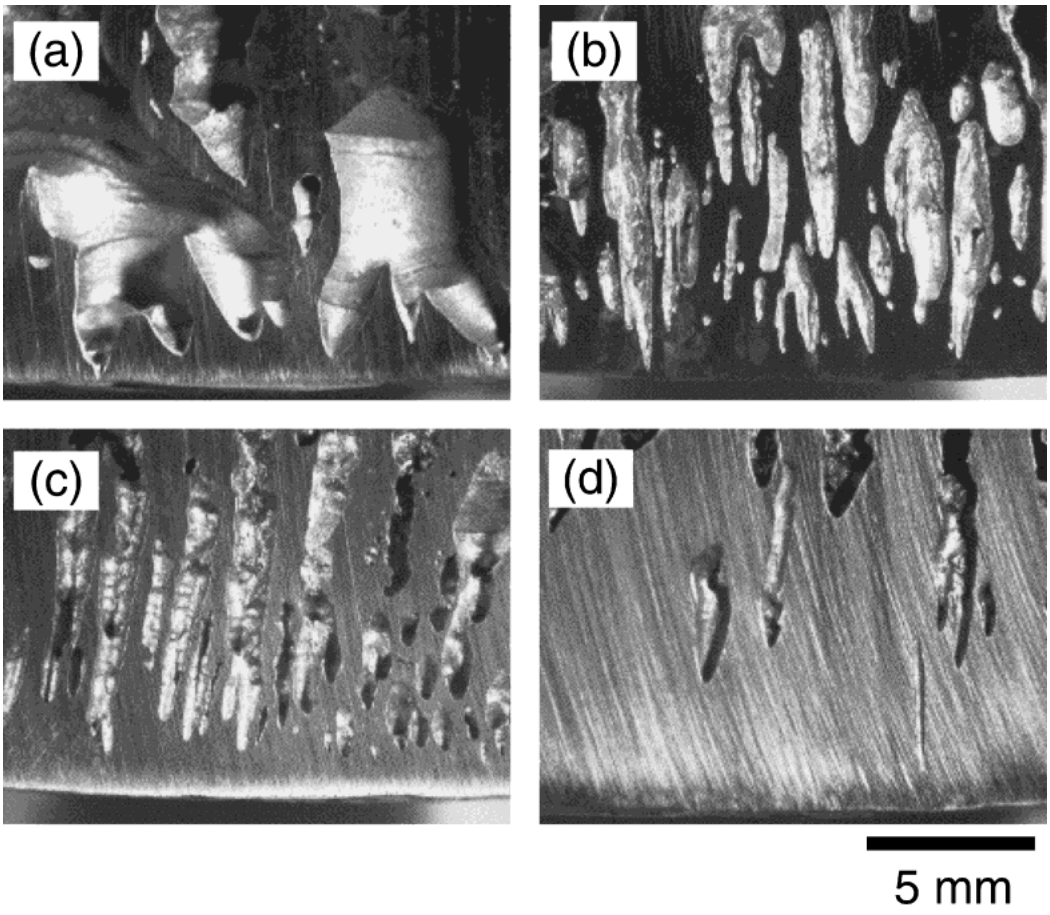

Fig. 5 Cross sectional planes parallel to the solidification direction in the ingots cast under mixture gase of 0.6 MPa of hydrogen and (a) 0 MPa, (b) 0.6 MPa, (c) 1.0 MPa or (d) 1.4 MPa of argon.

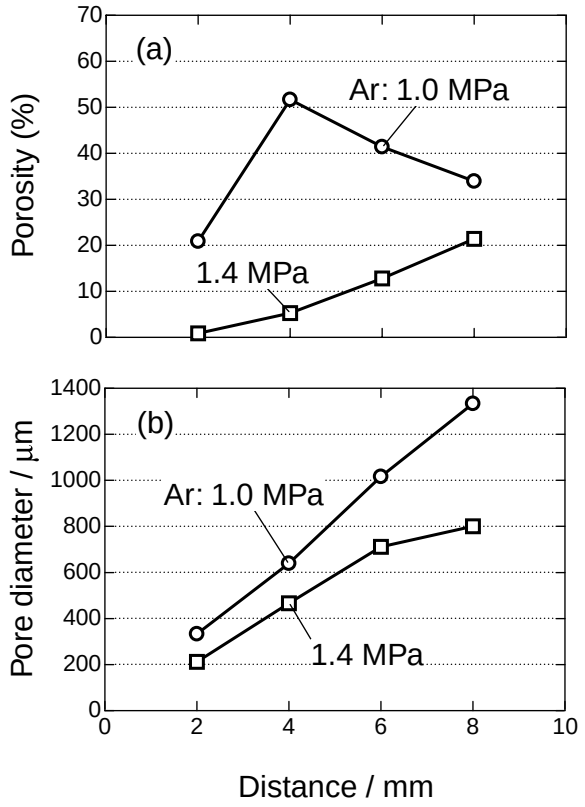

Fig. 6 Variation of (a) porosity and (b) averaged pore diameter with the distance from the bottom plane in the ingots cast under the mixed gases of 0.6 MPa of hydrogen and 1.0 or 1.4 MPa of argon.

argon. Both average pore diameter and porosity are larger in sample C. Generally, the solubility of hydrogen in metals and alloys follows the Sieverts' law,

$$C = kp^{1/2}, \tag{1}$$

where C is the concentration of hydrogen atoms in an alloy, k is the equilibrium constant and p is the hydrogen pressure. Therefore, it is expected that the concentrations of hydrogen in the liquid state of samples A, B, C and D and hence the molar quantities of hydrogen that form pores in these samples are not different since the hydrogen pressures are constant. On the other hand, the pressure of hydrogen gas in pores, p_{H_2}, should be balanced with the total pressure, $p_{H_2} + p_{Ar}$. Under a constant partial pressure of hydrogen, $p_{H_2,1}$ ($=p_{H_2,2}$), this results in the smaller volume of pores, V_2 ($<V_1$), in the samples cast under the higher partial pressure of argon, $p_{Ar,2}$ than under the lower partial pressure of argon, $p_{Ar,1}$, according to Boyle's law,

$$(p_{H_2,1} + p_{Ar,1})V_1 = (p_{H_2,2} + p_{Ar,2})V_2. \tag{2}$$

This is considered to be the reason for the lower porosity in sample D compared with sample C.

3.3 Effect of partial pressure of hydrogen on porosity

Figure 7 shows the cross sections perpendicular to the solidification direction at 2 mm from the bottom plane in the samples fabricated under various combinations of hydrogen and argon partial pressures with total pressure of 2.0 MPa. It is found that the number density of pores and hence porosity

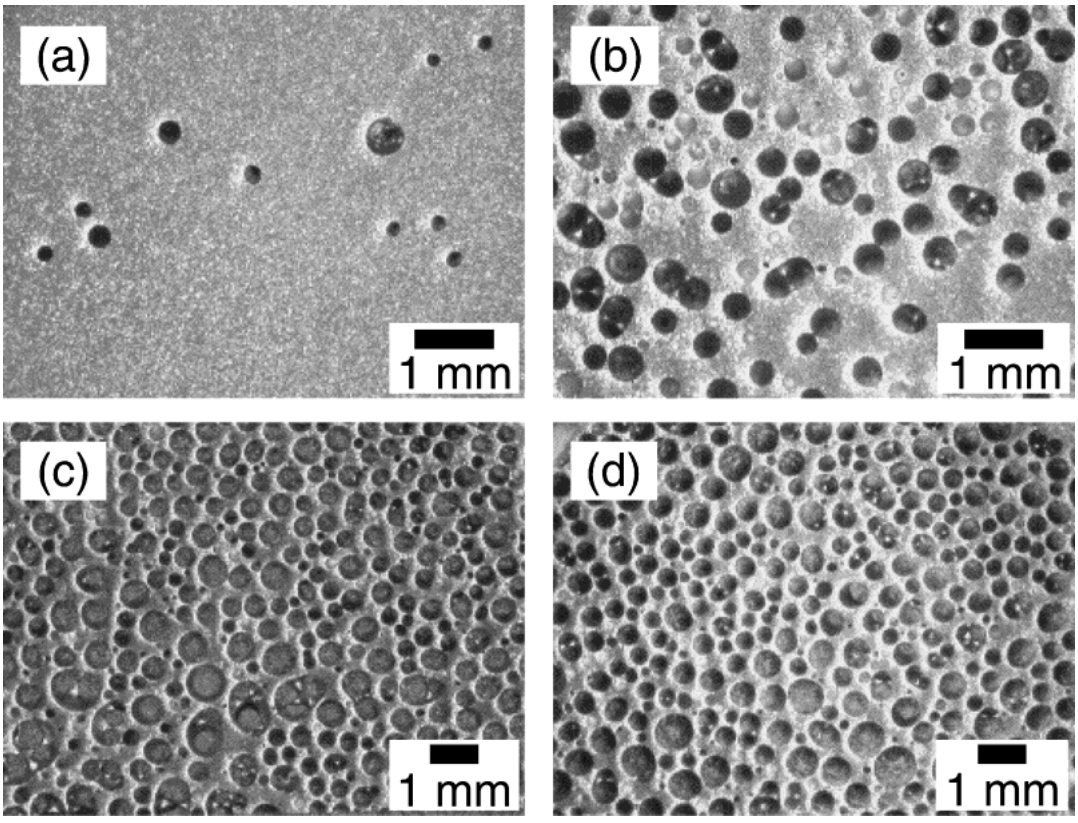

Fig. 7 Cross sectional plane perpendicular to the solidification direction at 2 mm from the bottom plane in the ingots cast under the mixed gases of (a) 0.6 MPa of hydrogen and 1.4 MPa of argon, (b) 0.8 MPa of hydrogen and 1.2 MPa of argon, (c) 1.0 MPa of hydrogen and 1.0 MPa of argon or (d) 1.2 MPa of hydrogen and 0.8 MPa of argon.

increase with increase of partial pressure of hydrogen. The hydrogen pressure in pores, which should be balanced with the total pressure, in porous metals fabricated under the same total pressure are expected to be the same even if the partial pressures of hydrogen are different. In this case, the porosity depends on the solubility of hydrogen, which is expressed by eq. (1). Therefore, it is reasonable that the porosity is larger in samples fabricated under higher partial pressure of hydrogen.

Figure 8 shows the porosity and average pore diameter as functions of the distance from the bottom plane determined by analysing the cross sections perpendicular to the solidification direction in the samples fabricated under constant total pressure of 2.0 MPa. In entire region, it is found that the porosity is higher in the sample fabricated under higher partial pressure of hydrogen except for 2.0 MPa of partial pressure in the region of larger distance from the bottom plane. The cause of such an exception, which is considered to be related to the difference of cooling rate by the distance from the bottom plane, is discussed in the next section. While average pore diameter is larger in samples fabricated under higher partial pressure of hydrogen in the region near the bottom plane up to 2 or 4 mm, such a trend is not observed at the larger distance. Since the average pore diameter depends on argon pressure in samples under a constant hydrogen pressure of 0.6 MPa in Fig. 6, it seems that the average pore diameter depends mainly on total pressure.

Figure 9 shows the pressure dependence of the porosity determined averaging the porosities within the region where cylindrical pores are observed to extend parallel to the solidification direction. The porosity is higher in the samples fabricated using lower pressure of argon under a constant partial hydrogen pressure of 0.6 MPa and is also higher using higher partial pressure of hydrogen under a constant total pressure of 2.0 MPa. These pressure dependence of the porosity is understood in the light of the Sieverts' law and Boyle's law as mentioned above.

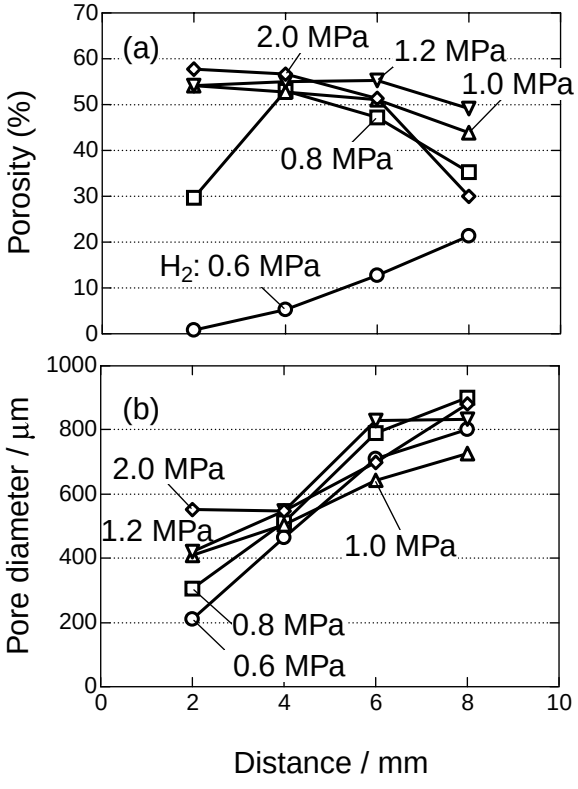

Fig. 8 Variation of (a) porosity and (b) averaged pore diameter with the distance from the bottom plane in the ingots cast under the mixed gases of hydrogen and argon, 0.6 MPa of hydrogen and 1.4 MPa of argon ('D'), 0.8 MPa of hydrogen and 1.2 MPa of argon ('F'), 1.0 MPa of hydrogen and 1.0 MPa of argon ('G') or 1.2 MPa of hydrogen and 0.8 MPa of argon ('H') or 2.0 MPa of hydrogen and 0 MPa of argon ('I'). Numerical values in the figures indicate the hydrogen partial pressure.

3.4 Influence of distance from the bottom plane

It is seen, in Figs. 6 and 8, that the average pore diameter increases with increase of the distance from the bottom plane. From Figs. 3(a) and 5, it is found that this is attributed to two causes; one is the growth of each pore, and another is the coalescence of more than one pores. The former one is considered to be due to the slower cooling rate at positions further from the bottom plane.

In Fig. 8, the porosity increases with increasing distance from bottom plane in the sample of hydrogen pressure of 0.6 MPa. This is due to increase of the pore diameter. However, in other atmosphere, the porosity decreases with increasing distance from bottom plane, while the average pore diameter increases. It is deduced that pores grow so large with the progress of solidification that the buoyant force working against the pores become large and the pores are not taken in solid but rise from the interface between solid and liquid to the liquid. The inflection of porosity curve of argon pressure of 1.0 MPa in Fig. 6 is also considered to due to the same cause.

In order to fabricate the porous stainless steels that have an uniform porosity or average pore diameter in the solidification direction, it is necessary to apply the solidification method by which a constant cooling rate is achieved.

3.5 Tensile tests

Figure 10(a) shows a picture of a sample cut out from in-

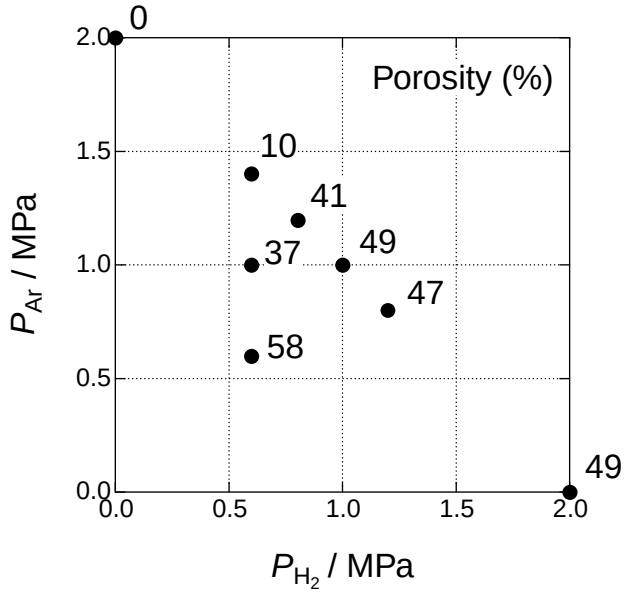

Fig. 9 Porosity (%) of porous stainless steel (SUS304L) fabricated under various couples of hydrogen and argon pressures. The number in the figure shows the porosity (%).

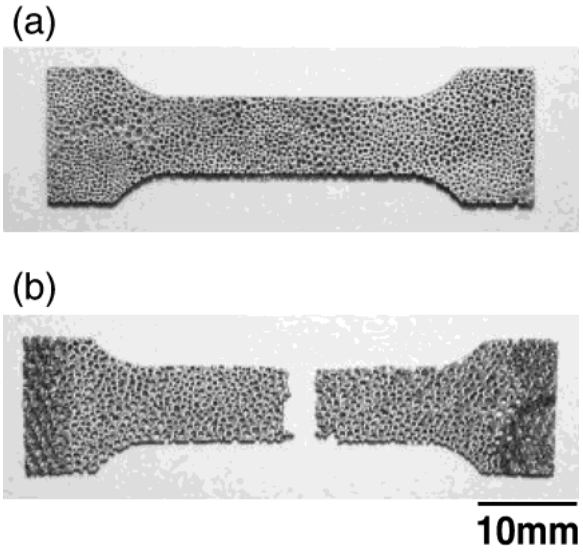

Fig. 10 A picture of specimen of porous stainless steel for a tensile test: (a) before a tensile test and (b) after fracture by a tensile test.

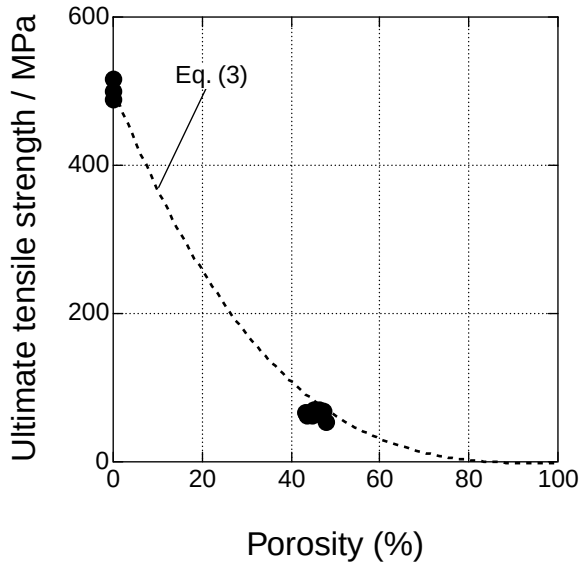

Fig. 12 Ultimate tensile strength of porous and stainless steel in the direction perpendicular to solidification direction as a function of porosity.

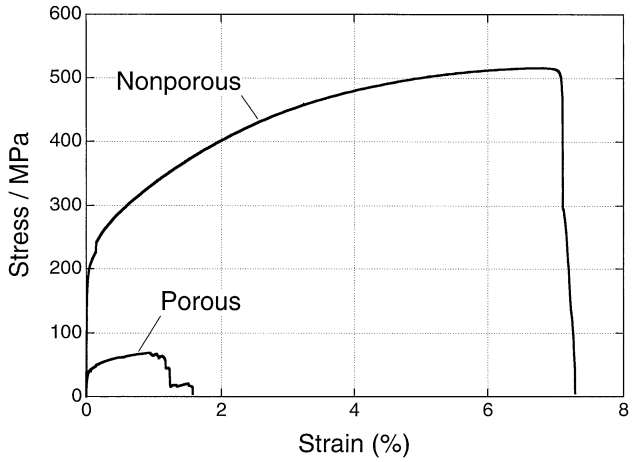

Fig. 11 Examples of stress-strain curves obtained from porous and nonporous stainless steel SUS304L.

got 'K'. The distribution of pores is almost homogeneous whose direction is perpendicular to the tensile directions. Figure 10(b) shows a sample after fracture. In this case the fracture occurred at the middle point in the sample.

Figure 11 is the stress-strain curve obtained from porous and nonporous samples. It is found that both elongation and ultimate tensile strength for nonporous alloy are both larger than those for porous alloy. Figure 12 shows the ultimate tensile strength in the direction perpendicular to the solidification direction. In the figure, the porosity is taken as the horizontal axis. The fraction of decrease in the ultimate tensile strength of the porous alloy to that of the nonporous alloy is larger than the fraction of decrease in the density. This is considered to be due to the stress concentration as well as in case of porous copper.[18] The dotted curve indicates the one expressed by the equation,

$$\sigma = \sigma_0(1 - \varepsilon/100)^K \quad (K = 3), \tag{3}$$

where σ is the strength of the specimen that has pores of ε (%) in volume fraction, σ_0 is the strength of nonporous specimen and K is the stress concentration coefficient. In porous copper, the ultimate tensile strength in the direction perpendicular to the pore direction is expressed well by eq. (3).[18] It is found that the ultimate tensile strength of the stainless steel (SUS304L) also follows eq. (3) in the present study. The solid part of the porous stainless steel can include hydrogen atoms than the nonporous one. However, the concentration of hydrogen atoms in solid part of the porous stainless steel is not considered to be so much that they influence on the mechanical property of the solid part of the porous stainless steel at room temperature.

4. Conclusions

Lotus-type porous stainless steel SUS304L has been fabricated by unidirectional solidification under mixed gases of hydrogen and argon. The porosity depends on the atmosphere pressure; it is lower using the higher partial pressure of argon under a constant partial pressure of hydrogen and is higher using higher partial pressure of hydrogen under a constant total pressure of atmosphere composing of hydrogen and argon. Average pore diameter increases with increasing distance from the bottom chill plane. This is due to the slower cooling rate at further distance from the bottom plane. From tensile tests, the ultimate tensile strength of porous alloy with porosity about 50% has been found to be by a factor of about 7 lower than nonporous alloy in the direction perpendicular to pore growth direction.

Acknowledgments

The present authors wish to thank Mr. Y. Nakai for his help in cutting samples by a spark-erosion wire-cutter. This work was supported by Grant-in-Aid for University and Society Collaboration (11792022) and Grant-in-Aid for Scientific Research on Priority Areas (A) (Protium 11135219) of the Ministry of Education, Culture, Sports, Science and Technology, Japan.

REFERENCES

1) V. A. Tracey: Int. J. Powder Metall. Powder Tech. **12** (1976) 25.
2) L. Albano-Muller: Powder Metall. Int. **14** (1982) 73.
3) *Handbook of Cellular Metals*, ed. H. P. Degischer and B. Kriszt (Wiley-VCH Verlag GmbH, Weinheim, 2002).
4) M. Imabayashi, M. Ichimura and Y. Kanno: Trans., JIM **24** (1983) 93–100.
5) I. Svensson and H. S. Fredriksson: Proc. Int. Conf. organized by the Applied Metallurgy and Metals Tech. Group of TMS, U. of Warwick, (1980) p. 376–380.
6) O. Knacke, H. Probst and J. Wernekinck: Z. Metallkde. **70** (1979) 1–6.
7) L. V. Boiko, V. I. Shapovalov and E. A. Chernykh: Metallurgiya **346** (1991) 78–81.
8) A. Pattnaik, S. C. Sanday, C. L. Vold and H. I. Aaronson: Mat. Res. Soc. Symp. Proc. **371** (1995) 371–376.
9) Y. Zheng, S. Sridhar and K. C. Russell: Mat. Res. Soc. Symp. Proc. **371** (1995) 365–370.
10) H. Nakajima: Mater. Integration **12** (1999) 37–44.
11) H. Nakajima: Boundary **15** (1999) 9–11.
12) H. Nakajima: Production Tech. **51** (1999) 60–62.
13) S. K. Hyun, Y. Shiota, K. Murakami and H. Nakajima: Proc. Int. Conf. on Solid-Solid Phase Transformations '99 (JIMIC-3), M. Koiwa, K. Otsuka and T. Miyazaki (Eds.), (Japan Inst. Metals, Kyoto, 1999) pp. 341–344.
14) H. Nakajima: J. High Temp. Soc. **26** (2000) 95–100.
15) H. Nakajima: Function Mater. **20** (2000) 27–34.
16) H. Nakajima, S. K. Hyun, K. Ohashi, K. Ota and K. Murakami: Colloids Surfaces A: Physicochem. Eng. Aspects **179** (2001) 209–214.
17) H. Nakajima: Bull. Iron Steel Inst. Japan **6** (2001) 701–707.
18) S. K. Hyun, K. Murakami and H. Nakajima: Mater. Sci. Eng. **A299** (2001) 241–248.
19) S. K. Hyun, K. Murakami and H. Nakajima: *Cellular Metals and Metal Foaming Technology*, ed. J. Banhart, M. F. Ashby and N. A. Fleck, (MIT, Verlag, 2001) pp. 421–424.
20) S. K. Hyun and H. Nakajima: *Cellular Metals and Metal Foaming Technology*, ed. J. Banhart, M. F. Ashby and N. A. Fleck (MIT, Verlag, 2001) pp. 181–186.
21) S. Yamamura, K. Murakami, H. Shiota and H. Nakajima: *Cellular Metals and Metal Foaming Technology*, ed. J. Banhart, M. F. Ashby and N. A. Fleck (MIT, Verlag, 2001) pp. 425–428.
22) S. Yamamura, H. Shiota, K. Murakami and H. Nakajima: Mater. Sci. Eng. **A318** (2001) 137–143.
23) H. Nakajima, S. K. Hyun and K. Murakami: Advanced Tech. Mater. **4** (2002) 13–18.
24) S. K. Hyun and H. Nakajima: Mater. Trans. **43** (2002) 526–531.
25) L. J. Gibson and M. F. Ashby: *Cellular Solids*, (2nd edition, Cambridge Univ. Press, 1997) pp. 1–14.
26) K. Ota, K. Ohashi and H. Nakajima: J. the JCBRA **40** (2001) 238–242.
27) Tekko Shinbun, 17 April (2002), Tekko Shinbun Corp., Tokyo.
28) T. Tanabe, Y. Yamanishi, K. Sawata and S. Imoto: J. Nucl. Mater. **122–123** (1984) 1568–1572.
29) S. Xiukui, X. Jian and L. Yiki: Mater. Sci. Eng. **A114** (1989) 179–187.
30) M. Mitra and K. W. Lange: Steel Res. **61** (1990) 353–358.